Progress in Oceanography 247 (2026) 103792

Contents lists available at ScienceDirect

Progress in Oceanography

journal homepage: www.elsevier.com/locate/pocean

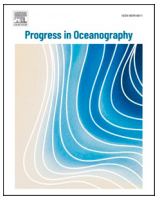

Microbial response to temperature and organic matter shifts in deep Antarctic sediments

G. Luongo [a,f], C. Corinaldesi [a,f], A. Dell'Anno [b,f], A. Giorgetti [b], A. Pusceddu [c], E. Rastelli [d], M. Tangherlini [e,f], A. Cau [c], C. Ennas [c], S. Greco [g], R. Danovaro [b,f,*]

[a] Department of Materials, Environmental Sciences and Urban Planning, Polytechnic University of Marche, Via Brecce Bianche, 60131 Ancona, Italy
[b] Department of Life and Environmental Sciences, Polytechnic University of Marche, Via Brecce Bianche, 60131 Ancona, Italy
[c] Department of Life and Environmental Sciences, University of Cagliari, Via T. Fiorelli 1, 09126 Cagliari, Italy
[d] Department of Marine Biotechnology, Stazione Zoologica "Anton Dohrn", Fano Marine Centre, Viale Adriatico 1-N, 61032 Fano, Italy
[e] Department of Research Infrastructures for Marine Biological Resources, Stazione Zoologica Anton Dohrn, Fano Marine Centre, Viale Adriatico 1-N, 61032 Fano, Italy
[f] National Biodiversity Future Centre, Palermo, Italy
[g] University of Gastronomic Sciences, Pollenzo, CN, Italy

ARTICLE INFO

Keywords:
Antarctica
Deep-sea ecosystems
Viral infections
Benthic prokaryotic diversity

ABSTRACT

The identification of the factors driving the biodiversity and metabolism of microbial components in deep-sea Antarctic ecosystems is crucial in light of their rapid transformations. Here, through a replicated and hierarchical sampling strategy, we investigated two deep-sea benthic areas in the Ross Sea (Antarctica) characterized by different bottom temperatures (ΔT ca. 1.3°C) and trophic conditions. The warmer and more oligotrophic deep seafloor showed higher bacterial and archaeal diversity and faster organic matter cycling, whilst the colder mesotrophic system displayed a higher organic matter content and microbial biomass. Proteobacterial assemblages dominated both areas, yet only 9.2% of the taxa were shared between the two sampling areas, indicating a major turnover in microbial biodiversity. Multiple linear regression models identified temperatures and organic matter as key drivers of prokaryotic assemblages and ecosystem functioning, with viral infections playing a potential role in organic matter cycling. These findings allow understanding how environmental changes in Antarctic benthic ecosystems, such as those potentially induced by climate change, could alter the biodiversity and metabolism of the microbial components and the organic matter cycling.

1. Introduction

Deep-sea life is typically 'food limited' as it largely depends on downward fluxes of the biomass produced in the surface ocean, which decreases exponentially with increasing water depth (Smith et al., 2008). Microbes represent the largest fraction of the total biomass in deep-sea sediments (Danovaro et al., 2015; Whitman et al., 1998) and are key drivers of organic matter (OM) cycling and nutrient regeneration (Danovaro et al., 2014).

Deep-sea ecosystem functioning and biogeochemical processes largely depend on the interplay between bottom-up and top-down controls: bottom-up controls include the quantity and quality of organic matter reaching the seafloor from surface production, which fuels benthic microbial metabolism and nutrient regeneration (Danovaro et al., 2016b; Walker et al., 2021), whereas top-down controls include predation and viral infections, which can regulate abundance, activity, and carbon transfer across trophic levels (Danovaro et al., 2008; Danovaro et al., 2016a).

In the Southern Ocean, primary productivity displays wide spatial–temporal changes, with phytoplankton blooms at the end of the austral spring in ice-free waters (Arrigo et al., 2008; Arteaga et al., 2020; Smith and Comiso, 2009). On the one hand, such variability depends on the temporal succession of several phytoplanktonic groups, which can bloom and decline over the short term (i.e., approximately two weeks) (Mangoni et al., 2018; Smith and Comiso, 2009). On the other hand, high local variability is due to the presence of specific environmental conditions, such as the presence of "polynyas", which are areas of ice-free open waters surrounded by ice, able to trigger seasonal phytoplankton blooms (Bolinesi et al., 2020; Mangoni et al., 2017; Smith et al., 2014; Smith and Comiso, 2009). Overall, these features

* Corresponding author.
E-mail address: r.danovaro@univpm.it (R. Danovaro).

https://doi.org/10.1016/j.pocean.2026.103792
Received 6 April 2025; Received in revised form 8 June 2026; Accepted 30 June 2026
Available online 2 July 2026

influence the temporal and spatial patterns of organic matter export to the deep Antarctic seafloor (>200 m water depth) (Chiarini et al., 2019; Langone et al., 2000).

There is considerable interest in understanding the interplay between climate change and its implications for the deep sea (Arneth et al., 2020). Climate change is expected to alter the thermal and trophic conditions of the Antarctic ecosystems (Queirós et al., 2024; Sweetman et al., 2017). Warmer temperatures are expected to increase ice melting (Jacobs et al., 2022; Silvano et al., 2020), lengthening the ice-free periods and enhancing primary production (Sweetman et al., 2017). This would finally lead to an increase in carbon export to the deep seafloor (Comiso, 2010; Jones et al., 2014; Sweetman et al., 2017). Changes in temperature and trophic conditions at the seafloor can alter microbial metabolic rates, potentially accelerating organic matter biogeochemical cycling with profound changes in ecosystem structure and functioning (Danovaro et al., 2017). In addition, viruses and prokaryotes are expected to react rapidly to changes in environmental conditions (Nomaki et al., 2021; Sweetman et al., 2019) either in terms of abundance, diversity, and metabolic rates, with potentially important implications for microbial dynamics and biogeochemical processes (Thullner and Regnier, 2019).

Here, we investigated spatial and temporal changes in deep-sea benthic prokaryotic diversity and viral infections in two Ross Sea systems characterized by different temperature and trophic conditions (Cerchierini et al., 2004; Langone et al., 2000). By comparing these contrasting systems, we aimed to assess differences in prokaryotic biodiversity and turnover in relation to temperature and trophic conditions, and to explore their potential response to environmental shifts and climate change.

2. Materials and methods

2.1. Study area and sample collection

Sediment samples were collected in the western part of the Ross Sea (Antarctica, 72-74°S; 174-175°E; Fig. S1) during the XXXII Italian Antarctic Expedition between January and February 2017. This region is characterized by a deep shelf with irregular topography containing high-relief banks and depressions, where the presence of the Drygalski Basin (1200 m depth canyon) isolates the shelf from the shore (Halberstadt et al., 2016), offering a pathway for cold bottom water to flow northwards (Smith Jr *et al.*, 2014). Samples were collected from 2 areas of the western Ross Sea, named Area B and Area C, located at ca. 200 km from each other.

Area B (average depth 586 m, 74°01′S, 175°04′E) is located in the northern part of the JOIDES Basin and was characterized by biosiliceous muddy sediments (Capotondi et al., 2020). Here, the Modified Circumpolar Deep Water (forming from the mixing of the Circumpolar Deep Waters and shelf waters) intrudes into the continental shelf along the east side of the JOIDES basin and mixes near the bottom with the High Salinity Shelf Water (Orsi and Wiederwohl, 2009). The High Salinity Shelf Water is the densest water mass in the Southern Ocean, which moves northward following clockwise circulation, creating water conditions characterized by high salinity (> 34.7) and temperatures close to the freezing surface point (about − 1.92°C) (Jacobs et al., 1985; Rivaro et al., 2014).

Area C (average depth 432 m, 72°30′S, 174°56′E) is closer to the shelf break on the northern flank of the Mawson Bank, and is characterized by low surface water productivity, low sedimentation rates, and strong currents reaching 10–25 cm s^{-1} (Capotondi et al., 2020; Cerchierini et al., 2004).

The sampling strategy followed a replicated hierarchical design for capturing spatial and temporal variability. At large spatial scale, we compared two areas, Area B and Area C that are ~ 200 km apart. Within each area, two sub-areas were sampled, namely B1 and B2 (Area B) and C1 and C2 (Area C). These sub-areas were separated by approximately 2 km and were selected to assess mesoscale spatial variability within each area (Table S1). Each sub-area was sampled during two periods, hereafter referred to as sampling times T1 and T2, to assess short-term temporal changes in the investigated variables (Table S1). At all sampling sites and times, 3 independent replicates were collected. Sediment sampling was coupled with CTD casts in both periods to characterize bottom-water conditions. Sediment sampling was coupled with CTD casts to investigate bottom-water characteristics in both periods.

Sediment samples were collected using an oceanic box corer. At each station, sediments were obtained from 3 independent deployments of the box corer. Sediment sub-samples were then collected from each box corer using sterile Plexiglas tubes, and the top 1 cm of the sediment core was immediately processed for the analysis of viral and prokaryotic heterotrophic C production and extracellular enzymatic activities or stored at −20°C for the analysis of organic matter content and composition and prokaryotic abundance, biomass, and diversity.

2.2. Ocean assimilation model of total chlorophyll a concentration

Satellite data of chlorophyll *a* concentration (from January 2016 to January 2019) were downloaded from Copernicus Marine Service (CMEMS) database (https://doi.org/10.48670/moi-00281), a global dataset with a resolution of 4 × 4 Km, provided by the Copernicus Globcolour processor (Garnesson et al., 2019), and used here as a proxy of phytoplanktonic biomass to provide an indirect estimate of the amount of organic matter being produced through photosynthesis over time in the investigated Areas.

2.3. Sedimentary organic matter content and composition

Chlorophyll-a and phaeopigments in surface sediments were analyzed after extraction (12 h at 4°C, in the dark) using 90% (vol/vol) acetone (Lorenzen et al., 1980). After centrifugation, the supernatants were analyzed fluorometrically to estimate chlorophyll-a, and after acidification with 200 μL of 0.1 N HCl, to estimate the phaeopigments. The sum of chlorophyll-a and phaeopigment concentrations was expressed as chloroplastic pigment equivalents (CPE).

Total protein concentration (PRT) was analysed according to Hartree 1972 (Hartree, 1972), modified by Rice1982 (Rice, 1982). Total carbohydrate concentration was analysed according to Gerchakov and Hatcher (1972), optimized for sediment samples. Total lipids were extracted in chloroform: methanol (1:1, vol: vol(Bligh and Dyer, 1959)), and the resultant fraction, after evaporation in a dry hot bath (80-100°C for 20 min), was quantified spectrophotometrically after addition of H_2SO_4 (Marsh and Weinstein, 1966). Protein, carbohydrates, and lipid concentrations were expressed as bovine serum albumin, glucose, and tripalmitin, respectively, and the sum of their concentrations was converted into carbon equivalents (by using the conversion factors of 0.49, 0.40, and 0.75 mg C mg^{-1}, respectively) was defined as biopolymeric carbon (Danovaro, 2009).

2.4. Extracellular enzymatic activities and organic matter turnover

The aminopeptidase and β-glucosidase activities were determined by the analysis of the cleavage rates of the fluorogenic substrates L-leucine-4-methylcoumarinyl-7-amide (Leu-MCA) and 4-methylumbelliferyl (MUF)-b-D-glucopyranoside (Glu-MUF), respectively (Sigma Chemicals) under saturating substrate concentrations (Danovaro, 2009). Samples were incubated in the dark at *in situ* temperature for 1 h. The fluorescence of the samples was measured fluorometrically (380:440 nm, excitation: emission, for Leu-MCA and 365:455 nm, excitation: emission for Glu-MUF) immediately after the addition of the substrate and after the incubation and converted into enzymatic activity using standard curves of 7-amino-4-methylcoumarin for Leu-MCA and 4-methylumbelliferone for Glu-MUF (Sigma Chemicals).

Aminopeptidase and β-glucosidase activities were then used to

estimate the potential degradation rates of proteins and carbohydrates, respectively. The turnover times of these molecules were calculated as ratio between their amount and the rates of their degradation, and represent a measure of their cycling. For this calculation, protein and carbohydrate concentrations were first converted into carbon equivalents in order to estimate the amount of carbon contained in the sedimentary protein and carbohydrate pool (Danovaro, 2009). Protein carbon was obtained by multiplying protein concentrations, expressed as mg protein g^{-1} dry sediment, by a conversion factor of 0.49 mg C mg^{-1} protein, whereas carbohydrate carbon was obtained by multiplying carbohydrate concentrations, expressed as mg carbohydrate g^{-1} dry sediment, by a conversion factor of 0.40 mg C mg^{-1} carbohydrate (Danovaro, 2009). Also enzymatic activities were converted into carbon mobilization rates, assuming that 1 nmol of enzymatically hydrolysed substrate corresponds to 72 ng of mobilized C, and rates were expressed on a daily basis. Protein turnover time was therefore calculated by dividing the protein carbon pool by the aminopeptidase-derived daily carbon mobilization rate, whereas carbohydrate turnover time was calculated by dividing the carbohydrate carbon pool by the β-glucosidase-derived daily carbon mobilization rate. Shorter turnover times indicate faster potential degradation of the corresponding organic matter pool.

Aminopeptidase and β-glucosidase activities were also normalized per number of cells to evaluate the individual cell rates of substrate degradation.

2.5. Prokaryotic abundance, biomass, and heterotrophic C production

Prokaryotic abundances in the sediments were determined by epifluorescence microscopy, according to Danovaro (2009). To determine the prokaryotic biomass, prokaryotic size was converted into biovolume following inter-calibration by scanning electron microscopy (Danovaro, 2009). Prokaryotic heterotrophic C production was measured through the assessment of incorporation rates of ^{3}H-leucine (0.2 nmol final concentration, specific activity of 120.3 Ci $mmol^{-1}$) (Danovaro, 2009). The turnover time of prokaryotic biomass was used as a proxy for the potential renewal time of the benthic prokaryotic biomass. It was calculated by dividing prokaryotic biomass by heterotrophic C production, after converting biomass values from μg C g^{-1} to ng C g^{-1} to match the units of production, expressed as ng C $g^{-1}h^{-1}$. The resulting turnover time was expressed in hours, with shorter values indicating faster potential renewal of prokaryotic biomass.

2.6. Viral abundance and production

The abundance of viruses was determined by epifluorescence microscopy using the fluorochrome SYBR Gold (diluted till to a 2 × final concentration; (Danovaro, 2009). Viral production was determined using the dilution-based approach (Dell'Anno et al., 2009) which allows estimating the increase of viruses over time.

2.7. DNA extraction, purification, and sequencing

DNA was extracted and purified from the sediments using the Dneasy PowerSoil Kit (QIAGEN) with some modifications provided in Danovaro 2010 (Danovaro, 2009) for the removal of extracellular DNA. For the analysis of prokaryotic diversity, the 16S RNA gene was amplified using the primer set 515F-Y (5′-GTGYCAGCMGCCGCGGTAA) and 926R (5′-CCGYCAATTYMTTTRAGTTT) (Parada et al., 2016) and the amplicons sequenced on Illumina MiSeq platform by LGC group (Berlin, Germany) following Earth Microbiome Project protocols (https://www.earthmicrobiome.org/emp-standard-protocols/). Paired-end sequences were subsequently analyzed through the DADA2 procedure, as implemented within the QIIME2 pipeline (Bolyen et al., 2019) to infer biologically significant Amplicon Sequence Variants (ASVs). The resulting ASVs were then compared against the SILVA 16S database (v138) (Quast et al., 2012) for taxonomic affiliation using the VSEARCH-based inference plugin within QIIME2 (Bolyen et al., 2019) after trimming the reference sequences to the region amplified by the primers. The ASV table resulting from the DADA2 computation was refined to remove chloroplast- and mitochondrion-affiliated sequences and unclassified sequences before subsequent analyses.

Before the computation of alpha- and beta-diversity indices, the ASV table was rarefied to 15,000 sequences (corresponding to the number of sequences of the sample with the lowest sequence abundance, rounded down). The main alpha-diversity indices (i.e., ASV richness, Shannon index, and evenness) were calculated through the QIIME2 core-metrics plugin, together with the main beta-diversity calculations (e.g., Bray-Curtis distance). In addition to these indices, the non-rarefied ASV table was subjected to analysis through the DEICODE plugin (Martino et al., 2019), which produced a sample distance matrix based on the Aitchison distance (Gloor et al., 2017) to assess the differences in terms of ASV abundances.

Taxonomic inference of ASVs was carried out on the rarefied table to obtain a view of the assemblage structure at the family level (considering families contributing at least 0.5% to the whole assemblage and merging the remaining taxa into a single “Others” group).

2.8. Statistical analyses

To ascertain differences in the investigated variables between areas, sub-areas, and sampling times, permutational analyses of variance (PERMANOVA) (Anderson, 2014; Anderson and Millar, 2004) were carried out in either the univariate (variable by variable) and multivariate contexts. Details on PERMANOVA design and analyses are reported in the Supplementary Information.

Multiple linear regression models were fitted separately for each response variable, including prokaryotic abundance, heterotrophic C production, viral abundance and production, aminopeptidase and β-glucosidase activity, and observed ASVs as response variables. Before model fitting, the (multi)collinearity among candidate predictor variables was assessed using the Pearson Correlation Coefficient and the Variance Inflation Factor (VIF). Because of high (multi)collinearity, data regarding seafloor depth and bottom seawater salinity were excluded from the model selection procedure (Fig. S2). Since biopolymeric C and bottom water temperature were also highly correlated, they were not included in the same model; instead, separate candidate models were built considering either biopolymeric C or bottom water temperature as predictors, in order to retain both variables in the model-selection framework (Table 1). For each response variable, a set of candidate models was built using combinations of environmental and biological predictors considered relevant for the specific ecological relationship being tested. Moreover, the set of covariates was not fixed across all models, and some variables were used as response variables in some models and as predictors in others, such as prokaryotic abundance (Table 1).

Model selection was based on Akaike's information criterion (AIC). Between the candidate models, we selected the model with the lowest AIC in which all retained predictors were statistically significant ($p < 0.05$).

The selected models were then tested using the “model validation” procedure (Zuur and Ieno, 2016). The models were considered acceptable only when the residual *vs* fitted values did not show clear patterns, indicating homogeneity of variance and the independence of the predicted values. In addition, residuals were required to follow a normal distribution. The analyses were carried out using two complementary approaches: a *pooled approach,* in which all the samples were analysed together to identify common patterns, and a *not pooled* approach, in which Area B and Area C were analysed separately to identify “area-specific” relationships. Only models that successfully passed the model validation process and showed statistically relevant results were reported (Zuur and Ieno, 2016). For each selected model, the main

Table 1
Summary of the selected multiple linear regression models identifying the main environmental and biological predictors of prokaryotic, viral, and functional variables in Antarctic deep-sea sediments. For each model, the table reports the modelling approach, response variable, predictors, direction of the relationship (positive, +, and negative, −), statistical significance, explained variance (R^2), and Akaike's Information Criterion (AIC). The modelling approach indicates whether the model was fitted using all samples together (*pooled* approach) or separately for Area B and Area C (*not pooled* approach). Complete model outputs, including candidate predictors, regression coefficients, standard errors, and exact p-values, are provided in Table S4.

Approach	Response variable	Predictors	Relationship	Significance	R^2	AIC
Pooled	Prokaryotic abundance	Biopolymeric C	+	$p < 0.001$	0.48	904.7
Pooled	Heterotrophic carbon production	PRT/CHO	+	$p < 0.05$	0.756	275.8
		Viral Production	+	$p < 0.001$		
Pooled	Aminopeptidase activity	Biopolymeric C	−	$p < 0.01$	0.34	238.4
Pooled	Aminopeptidase activity	Bottom Water Temperature	+	$p < 0.01$	0.374	237.2
Pooled	Aminopeptidase activity	Proteins	−	$p < 0.01$	0.291	240.1
Pooled	β-glucosidase activity	Viral Production	+	$p < 0.001$	0.542	−23.68
Pooled	Viral abundance	Prokaryotic Abundance	+	$p < 0.01$	0.854	966.5
		Heterotrophic C Production	+	$p < 0.001$		
Pooled	Viral abundance	Biopolymeric C	+	$p < 0.01$	0.866	964.5
		Heterotrophic C Production	+	$p < 0.001$		
Pooled	Viral production	Heterotrophic C Production	+	$p < 0.001$	0.7	830.8
Pooled	Observed ASVs	Biopolymeric C	−	$p < 0.01$	0.483	215.2
Not Pooled − Area B	Heterotrophic carbon production	PRT/CHO	+	$p < 0.05$	0.62	137.4
		Viral Production	+	$p < 0.05$		
Not Pooled − Area B	Aminopeptidase activity	Bottom Water Temperature	+	$p < 0.05$	0.574	98.86
		Viral Production	+	$p < 0.05$		
Not Pooled − Area B	Aminopeptidase activity	Prokaryotic Abundance	+	$p < 0.05$	0.373	101.5
Not Pooled − Area B	β-glucosidase activity	Prokaryotic Abundance	−	$p < 0.001$	0.869	−20.1
		Viral Production	+	$p < 0.001$		
		PRT/CHO	+	$p < 0.01$		
Not Pooled − Area B	Viral abundance	Prokaryotic Abundance	+	$p < 0.01$	0.6	488.7
		Bottom Water Temperature	−	$p < 0.05$		
Not Pooled − Area B	Viral abundance	Prokaryotic Abundance	+	$p < 0.05$	0.715	486.7
		Heterotrophic C Production	+	$p < 0.01$		
		Biopolymeric C	+	$p < 0.05$		
Not Pooled − Area B	Viral production	Prokaryotic Abundance	+	$p < 0.05$	0.742	415.9
		Heterotrophic C Production	+	$p < 0.01$		
		PRT/CHO	−	$p < 0.05$		
Not Pooled − Area B	Viral production	Prokaryotic Abundance	+	$p < 0.001$	0.963	394.7
		Heterotrophic C Production	+	$p < 0.001$		
		Biopolymeric C	+	$p < 0.001$		
		PRT/CHO	−	$p < 0.001$		
Not Pooled − Area B	Observed ASVs	Biopolymeric C	−	$p < 0.05$	0.501	84.76
Not Pooled − Area C	Heterotrophic carbon production	Biopolymeric C	+	$p < 0.01$	0.644	105.9
Not Pooled − Area C	Heterotrophic carbon production	Prokaryotic Abundance	+	$p < 0.001$	0.943	85.89
		Bottom Water Temperature	+	$p < 0.01$		
Not Pooled − Area C	Aminopeptidase activity	Bottom Water Temperature	−	$p < 0.001$	0.917	99.74
		Prokaryotic Abundance	+	$p < 0.001$		
		Viral Production	+	$p < 0.01$		
		PRT/CHO	+	$p < 0.05$		
Not Pooled − Area C	Aminopeptidase activity	Prokaryotic Abundance	+	$p < 0.05$	0.958	89.63
		Viral Production	−	$p < 0.01$		
		Proteins	+	$p < 0.001$		
Not Pooled − Area C	β-glucosidase activity	Prokaryotic Abundance	+	$p < 0.01$	0.675	−30.62
		Viral Production	+	$p < 0.05$		
Not Pooled − Area C	Viral abundance	Prokaryotic Abundance	+	$p < 0.01$	0.508	461.6
Not Pooled − Area C	Viral abundance	Biopolymeric C	+	$p < 0.01$	0.701	457.6
		PRT/CHO	+	$p < 0.05$		
Not Pooled − Area C	Observed ASVs	Biopolymeric C	−	$p < 0.05$	0.722	106.8
		Proteins/Carbohydrates	−	$p < 0.05$		

information needed to interpret the regression analyses, including response variable, modelling approach, candidate predictors, retained significant predictors, direction of the relationships, p-values, R-squared values, and AIC values, is summarized in Table 1. The complete model outputs, including regression coefficients and standard errors, are reported in Table S4. All the statistical analyses were performed in Python v3.10 through *pandas* and *statsmodels* packages (McKinney, 2011).

To identify potential drivers of prokaryotic composition in the investigated Areas, non-parametric multivariate multiple regression analyses, based on Bray-Curtis similarity matrix, were carried out using the routine DISTLM forward selection procedure and AIC as the selection criterion(McArdle and Anderson, 2001) for the two Areas together (*pooled* approach) and for Area B and Area C separately (*not pooled* approach). Autocorrelated variables were removed from the DISTLM analyses (Fig. S2); as for univariate multiple linear regression analyses, temperature and biopolymeric C were considered separately.

3. Results

3.1. Environmental characteristics

Bottom-water salinity was 34.7 in Area B and 34.6 in Area C; bottom-water temperatures were lower in Area B (−1.8°C) than in Area C (−0.50°C to 0.04°C). Surface chlorophyll *a* concentration estimated from satellite images in Area B (1.6 ± 0.8 mg m^{-3}) was consistently higher than that in Area C (0.4 ± 0.2 mg m^{-3}) during the sampling periods and during the austral summer of the previous (2016) and following (2018) year (Fig. 1a). Such differences were reflected by sedimentary CPE concentrations, which in Area B (4.3 ± 0.3 μg g^{-1}) were about one order of magnitude higher than those in area C (0.3 ±

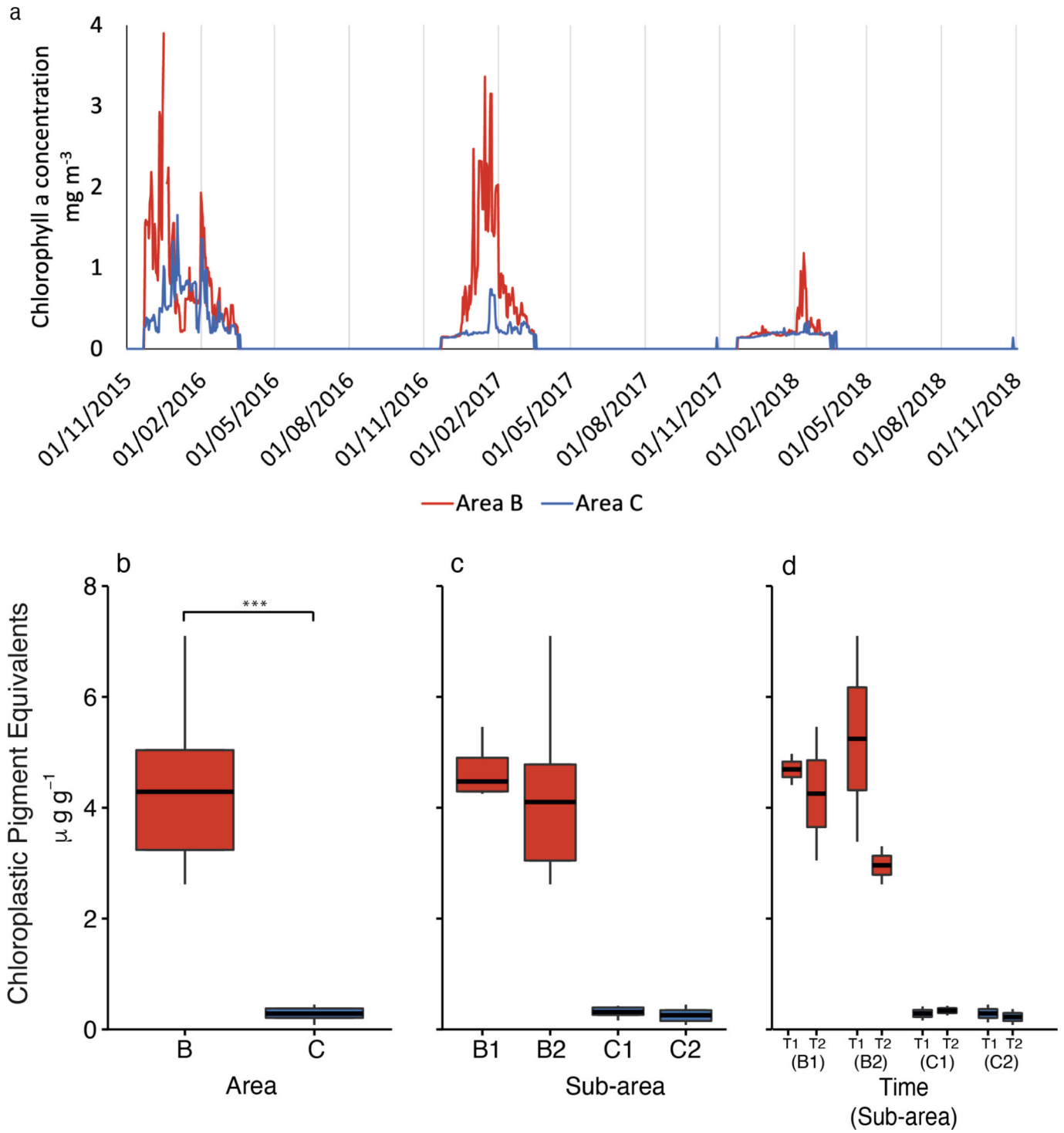

Fig. 1. Spatial and temporal variations of surface primary production and sedimentary phytopigments contents in the two investigated areas. The image (a) illustrates the amount of chlorophyll *a* concentration (mg m^{-3}) from January 2016 to January 2019 of the two sampling areas (https://doi.org/10.48670/moi-00281). The plots (b, c, d) show the concentrations of phytopigments comparing the values between the two areas (b), between sub-areas within each area (c), and between sampling times within each sub-area (d); reported are average values and standard deviations, with asterisks and brackets indicating significant differences found in the pairwise comparisons of PERMANOVA tests (***, $p < 0.001$; **, $p < 0.01$; *, $p < 0.05$).

0.01 µg g^{-1}; $p < 0.001$; Fig. 1b). In each of the two areas, no significant differences were found in CPE sedimentary contents between sub-areas, nor between sampling times in each sub-area (Fig. 1c-d).

Results of the PERMANOVA analyses carried out to ascertain differences in organic matter contents, biochemical composition, and nutritional quality between areas, sub-areas, and sampling times are reported in Tables S2 and S3. In both areas, all sub-areas, and sampling times, carbohydrates represented the main fraction (39–52%) of the BPC. Carbohydrate sedimentary contents in Area B (6.0 ± 0.6 mg g^{-1}) were > 3 times higher than in C (1.7 ± 0.4 mg g^{-1}; $p < 0.001$Fig. 2a). In both areas, carbohydrate content of the sediments did not show significant differences between sub-areas (Fig. 2b). In the sub-areas B1, B2 and C2, carbohydrate contents varied inconsistently over time ($p < 0.01$), whereas in the sub-area C1 they remained almost constant

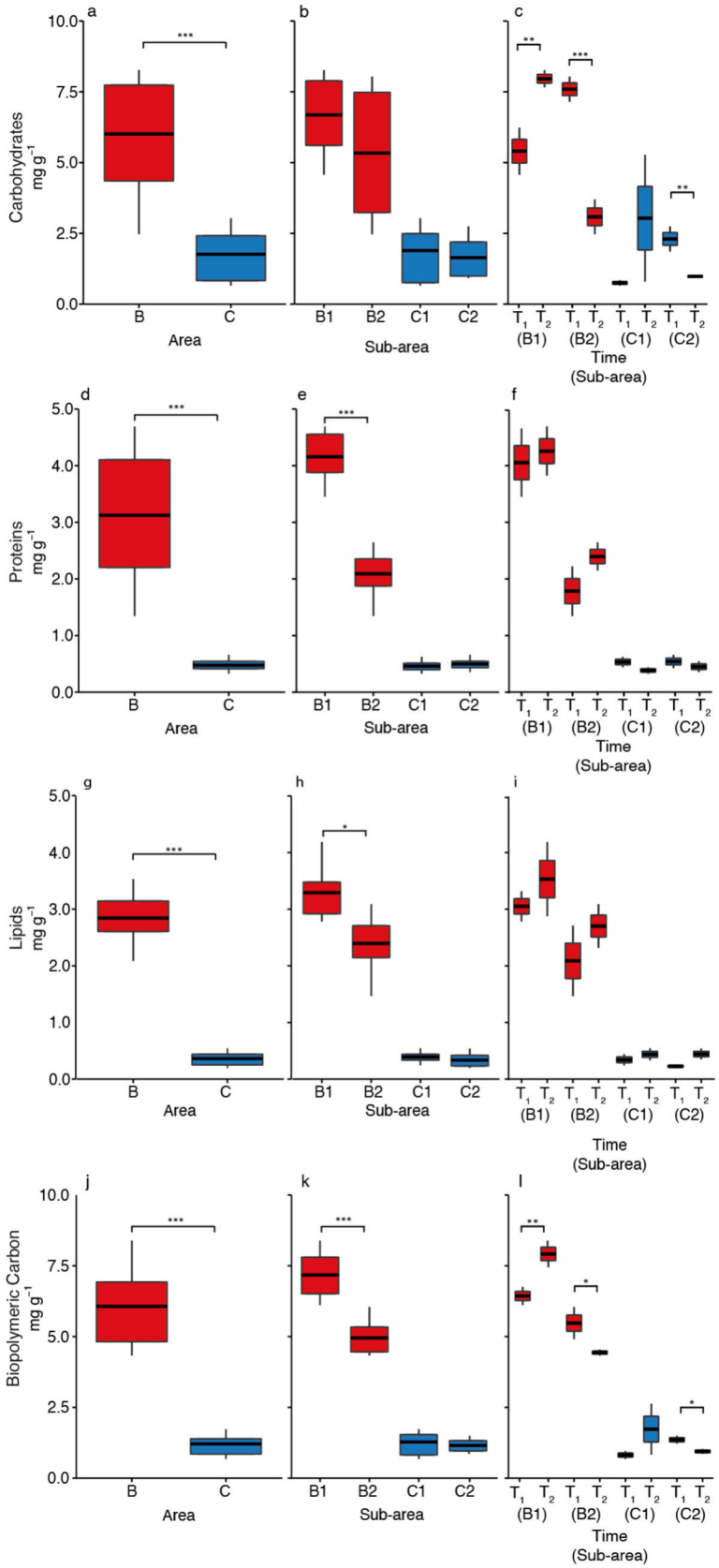

Fig. 2. Spatial and temporal variations of biopolymeric carbon, carbohydrate, protein and lipid contents in the sediments of the two investigated areas. The plots compare the carbohydrate, protein, lipid and biopolymeric carbon (BPC) contents in the two Areas (a, d, g, j), the two sub-areas within each area (b, e, h, k), and during the two sampling times within each sub-area (c, f, i, l). Data are expressed as mg of C per gram of dry sediments and are reported as average values and standard deviations, with asterisks and brackets indicating significant differences found in the pairwise comparisons of PERMANOVA tests (***, $p < 0.001$; **, $p < 0.01$; *, $p < 0.05$).

between sampling times (Fig. 2c).

Protein content of the sediments was 6.5 times higher in Area B (3.1 ± 0.34 mg g^{-1}) than in C (0.48 ± 0.03 mg g^{-1}; $p < 0.001$; Fig. 2d). Protein contents showed significantly higher values in the sub-area B1 than in B2 ($p < 0.001$), whereas values in the sub-areas C1 and C2 did not show significant differences (Fig. 2e). In all sub-areas, protein contents did not vary with sampling time (Fig. 2f). The protein-to-carbohydrate ratio (PRT/CHO) was always less than 1 (0.6 ± 0.2 in Area B *vs* 0.4 ± 0.2 in Area C).

Lipid content of the sediments was 7.9 times higher in Area B (2.8 ± 0.2 mg g^{-1}) than in C (0.4 ± 0.03 mg g^{-1}; $p < 0.001$; Fig. 2g). In Area B, lipid contents always showed significantly higher values in the sub-area B1 than in B2 ($p < 0.05$), whereas values did not differ significantly between sub-areas C1 and C2 (Fig. 2h). No differences were observed during the sampling period in the two areas (Fig. 2i).

The concentrations of biopolymeric C (BPC) were 5 times higher in Area B (6.1 ± 0.4 mg C g^{-1}) than in Area C (1.2 ± 0.2 mg C g^{-1}; $p < 0.001$; Fig. 2j). BPC contents varied between sub-areas in Area B ($p < 0.001$), but not in Area C (Fig. 2k). From T_1 to T_2, BPC contents changed significantly in sub-areas B1 ($p < 0.01$), B2 ($p < 0.05$), and C2 ($p < 0.05$), while they remained constant in sub-area C1 (Fig. 2l).

3.2. Prokaryotic abundance, biomass, and heterotrophic C production

Prokaryotic abundance was 3 times higher in Area B (1.0 ± 0.01 x10^8 cells g^{-1}) than in C (3.5 ± 0.94 x10^7 cells g^{-1}; $p < 0.001$; Fig. 3a). No significant differences were found in prokaryotic abundance between sub-areas within areas B or C (Fig. 3b). Significant differences among sampling times were found only in the sub-area B1, where values were higher at T_2 ($p < 0.01$; Fig. 3c).

The selected multiple linear regression models are summarized in Table 1, whereas complete model outputs, including regression coefficients and standard errors, are reported in Table S4.

The best model, using the *pooled* approach, indicated a positive relationship between prokaryotic abundance, as response, and biopolymeric C, as predictor, that explained 48% of the observed variation ($R^2 = 0.48$, $p < 0.001$, AIC = 904.7; Table 1).

Prokaryotic biomass was double in Area B (3.6 ± 0.3 μgC g^{-1}) than in C (1.4 ± 0.4 μgC g^{-1}; $p < 0.001$; Fig. 3d). Prokaryotic biomass in Area C was significantly higher in sub-area C1 than in C2 ($p < 0.05$), and a significant temporal variation was found only in the sub-area B2 ($p < 0.05$; Fig. 3e-f).

Prokaryotic heterotrophic C production showed values 10 times higher in Area B (255.3 ± 98.3 ngC $g^{-1}h^{-1}$) than in C (23.4 ± 29.5 ngC $g^{-1}h^{-1}$; $p < 0.001$; Fig. 3g). No significant differences were found between sub-areas (Fig. 3h) in both areas, and significant changes in the sampling period were found only in the sub-area B1 ($p < 0.01$; Fig. 3i).

The regression analyses, following the *pooled* approach, for the prokaryotic heterotrophic C production highlighted positive relationships with viral production coupled with the quality of organic substrates (expressed as protein to carbohydrate concentration ratio), explaining 76% of the variance ($R^2 = 0.756$; viral production, $p < 0.001$; PRT/CHO, $p < 0.05$; AIC = 275.8; Table 1). Considering the two Areas separately (*not pooled* approach), the best model suggested that the heterotrophic C production was correlated with viral production and organic matter quality in Area B, explaining together 62% of the variance ($R^2 = 0.620$; viral production, $p < 0.05$; PRT/CHO, $p < 0.05$; AIC = 137.4; Table 1). In the oligotrophic Area C, the best model showed a positive correlation with prokaryotic abundance and bottom-water temperature, explaining together 94% of the variance ($R^2 = 0.943$; prokaryotic abundance, $p < 0.001$; bottom-water temperature, $p < 0.01$; AIC = 85.89; Table 1).

Heterotrophic C production per cell showed values 3 times higher in Area B than in C (Fig. 3j; $p < 0.001$; Table 1), with no significant differences between sub-areas (Fig. 3k; Table 1). Heterotrophic C production per cell changed over time only in sub-area B1 ($p < 0.01$; Table 1), with a significant decrease at T_2 (Fig. 3l).

The turnover of prokaryotic biomass was 8 times faster in Area B than in C and did not differ between sub-areas in B, nor in C (Fig. S3a-c; $p < 0.01$; Table 1). Significant temporal variations were observed only in sub-areas B1 ($p < 0.01$) and C1 (Fig. S3c; $p < 0.01$; Table 1).

3.3. Extracellular enzymatic activities and organic matter turnover

At all the spatial and temporal scales investigated, aminopeptidase activity was always higher than β-glucosidase activity. Aminopeptidase activities (Fig. 4a-c) and aminopeptidase activities per cell (Fig. 4d-f) were lower in Area B than in C ($p < 0.001$; Table 1), and no significant differences were observed between sub-areas nor between sampling times in each sub-area.

The best multiple linear regression models, using the *pooled* approach, showed a positive correlation of aminopeptidase activity with bottom-water temperature, explaining alone 37% of the variance ($R^2 = 0.374$, $p < 0.01$, AIC = 237.2; Table 1). Conversely, taking into account organic matter concentration, we observed a negative relationship with biopolymeric C (explaining 34% of the variance in the model considering BPC; $R^2 = 0.340$, $p < 0.01$, AIC = 238.4; Table 1) and with proteins (29% of the variance in the model considering protein concentration; $R^2 = 0.291$, $p < 0.01$, AIC = 240.1; Table 1). The *not pooled* approach also revealed a positive relationship between aminopeptidase activities and bottom-water temperature together with viral production in Area B, which explained 57% of the variance ($R^2 = 0.574$; bottom-water temperature, $p < 0.05$; viral production, $p < 0.05$; AIC = 98.86; Table 1), while in Area C, aminopeptidase activities showed a positive relationship with PRT/CHO ratio, viral production, prokaryotic abundance, and a negative relationship with bottom-water temperature ($R^2 = 0.917$; prokaryotic abundance, $p < 0.01$; viral production, $p < 0.01$; PRT/CHO, $p < 0.05$; bottom-water temperature, $p < 0.001$; AIC = 99.74; Table 1). When protein concentration was considered in the model, aminopeptidase activity showed a positive correlation with prokaryotic abundance in Area B, explaining 37% of the variance ($R^2 = 0.373$, $p < 0.05$, AIC = 101.5; Table 1), while in Area C, aminopeptidase activity was correlated with prokaryotic abundance, viral production, and protein concentration, together accounting for 95% of the variance ($R^2 = 0.958$; prokaryotic abundance, $p < 0.05$; protein concentration, $p < 0.001$; viral production, $p < 0.01$; AIC = 89.63; Table 1).

Protein turnover times estimated in Area B were > 20 times slower than in Area C (Fig. 4g; $p < 0.001$; Table 1) and displayed significant differences only between sub-areas B1 and B2 ($p < 0.01$; Table 1). Significant temporal changes were observed only in sub-area B1, where the protein turnover time decreased from T_1 to T_2 (Fig. 4h, i; $p < 0.01$; Table 1).

β-glucosidase activities (Fig. 5a-c) were higher in Area B than in C ($p < 0.01$; Table 1), and no significant differences were observed between sub-areas in both areas. β-glucosidase activity per cell was higher in Area C than in Area B ($p < 0.05$; Table 1), and no significant differences were observed between sub-areas nor between sampling times in each sub-area (Fig. 5d-f). Potential carbohydrate turnover times were 2-fold slower in Area B than in C (Fig. 5g; $p < 0.001$; Table 1), and no differences were observed between sub-areas (Fig. 5h). In sub-area B1 and B2, carbohydrate turnover time changed significantly from T_1 to T_2 ($p < 0.01$; Table 1), whereas in Area C, no significant temporal variations in carbohydrate turnover time were observed (Fig. 5i).

The best multiple linear regression models, using the *pooled* approach, showed a positive correlation of β-glucosidase activities with viral production, explaining alone 54% of the variance ($R^2 = 0.542$, $p < 0.001$, AIC = − 23.68; Table 1). The *not pooled* approach revealed positive relationships of the β-glucosidase with viral production and a negative relationship with prokaryotic abundance in Area B, explaining 87% of the variance ($R^2 = 0.869$; viral production, $p < 0.01$; PRT/CHO, $p < 0.01$; prokaryotic abundance, $p < 0.001$; AIC = − 20.10; Table 1); in Area C, β-glucosidase activities showed positive relationships with viral

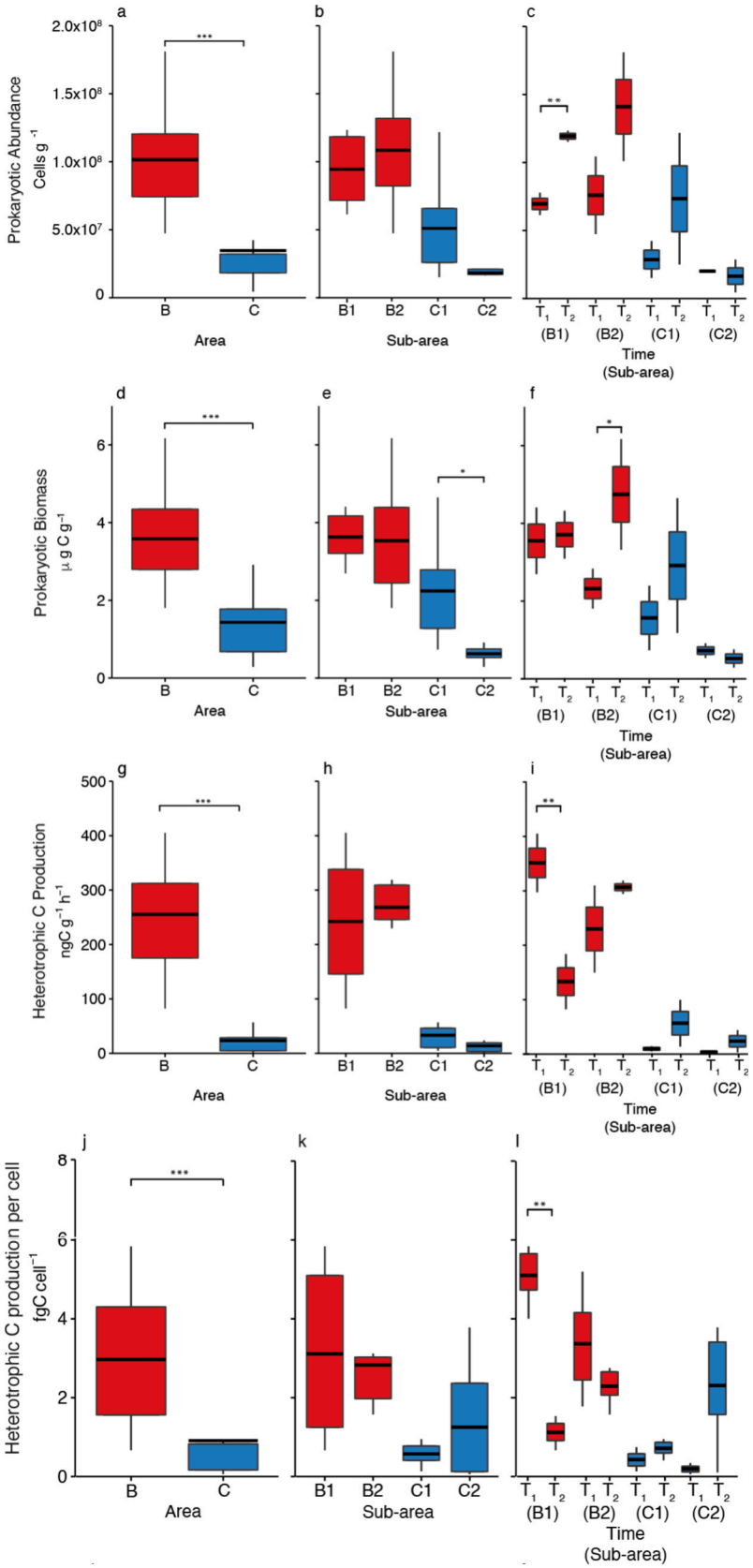

Fig. 3. Spatial and temporal variations of prokaryotic abundance, biomass, and heterotrophic C production and heterotrophic C production per cell in the sediments of the two investigated areas. The plots show the prokaryotic abundance (expressed as the number of prokaryotic cells per gram of dry sediments, cells g^{-1}), biomass (expressed as µg of C per gram of dry sediments, µgC g^{-1}), the heterotrophic C production (expressed as ng of C produced per gram of dry sediments per hour, ng C $g^{-1}h^{-1}$), and the heterotrophic C production per cell (expressed as fg of C produced per cell per hour, fg C cell-1 h-1) in the two Areas (a, d, g, j), in the two sub-areas

within each area (b, e, h, k), and during the two sampling times within each sub-area (c, f, i, l). Reported are average values and standard deviations, with asterisks and brackets indicating significant differences found in the pairwise comparisons of PERMANOVA tests (***, $p < 0.001$; **, $p < 0.01$; *, $p < 0.05$).

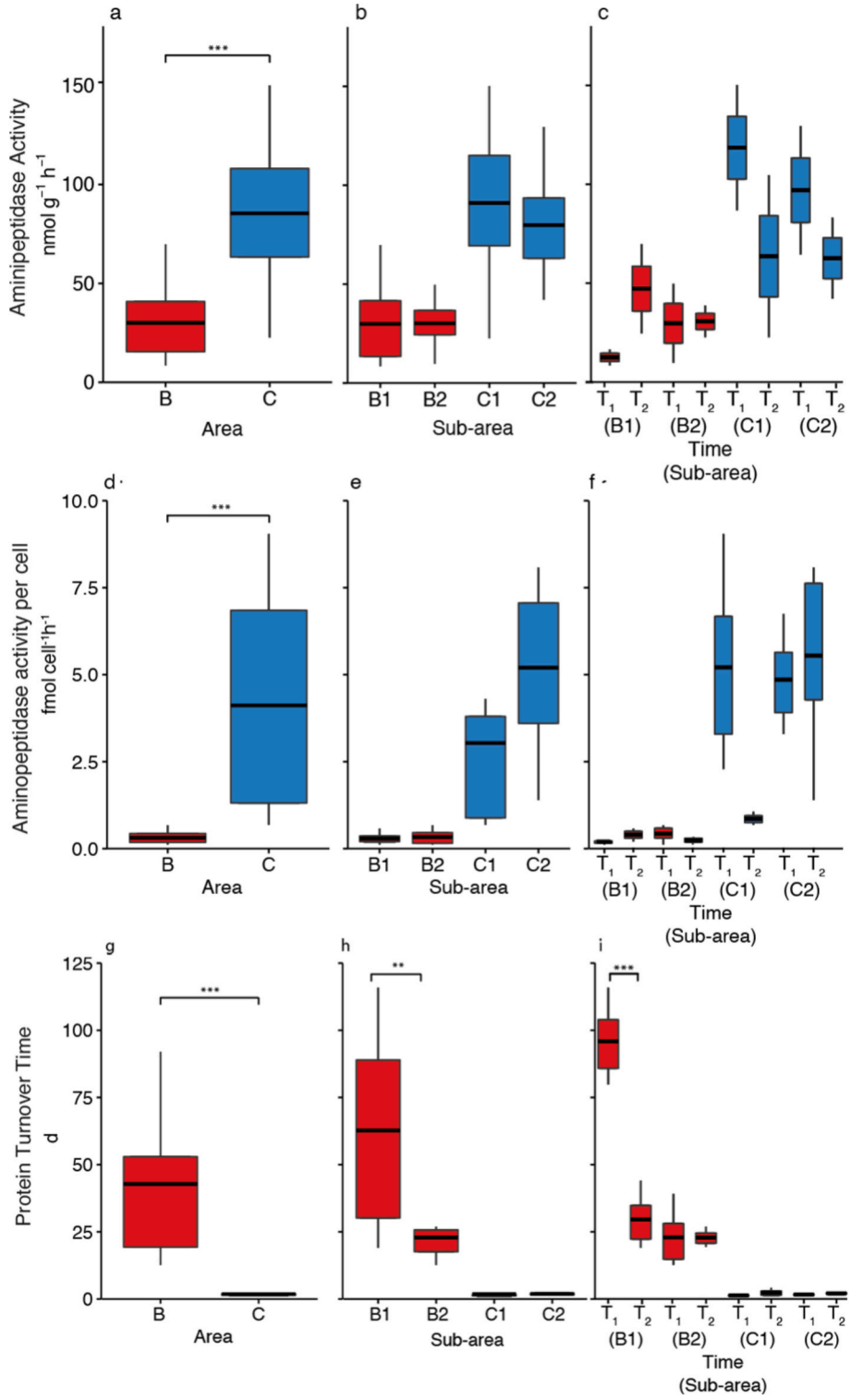

Fig. 4. Spatial and temporal variations of aminopeptidase activity, aminopeptidase activity per cell, and protein turnover time in the sediments of the two investigated areas. The plots show the aminopeptidase (expressed as nanomoles of nmol of C hydrolized per gram of dry sediment per hour, nmol $g^{-1}h^{-1}$), aminopeptidase activity per cell (expressed as fmol of C hydrolyzed per cell per hour, fmol $cell^{-1}h^{-1}$) and the protein turnover time (expressed as days, d) in the two Areas (a, d, g), in the two sub-areas within each area (b, e, h), and during the two sampling times within each sub-area (c, f, i). Reported are average values and standard deviations, with asterisks and brackets indicating significant differences found in the pairwise comparisons of PERMANOVA tests (***, $p < 0.001$; **, $p < 0.01$; *, $p < 0.05$).

production and prokaryotic abundance explaining together 68% of the variance ($R^2 = 0.675$; viral production, $p < 0.05$; prokaryotic

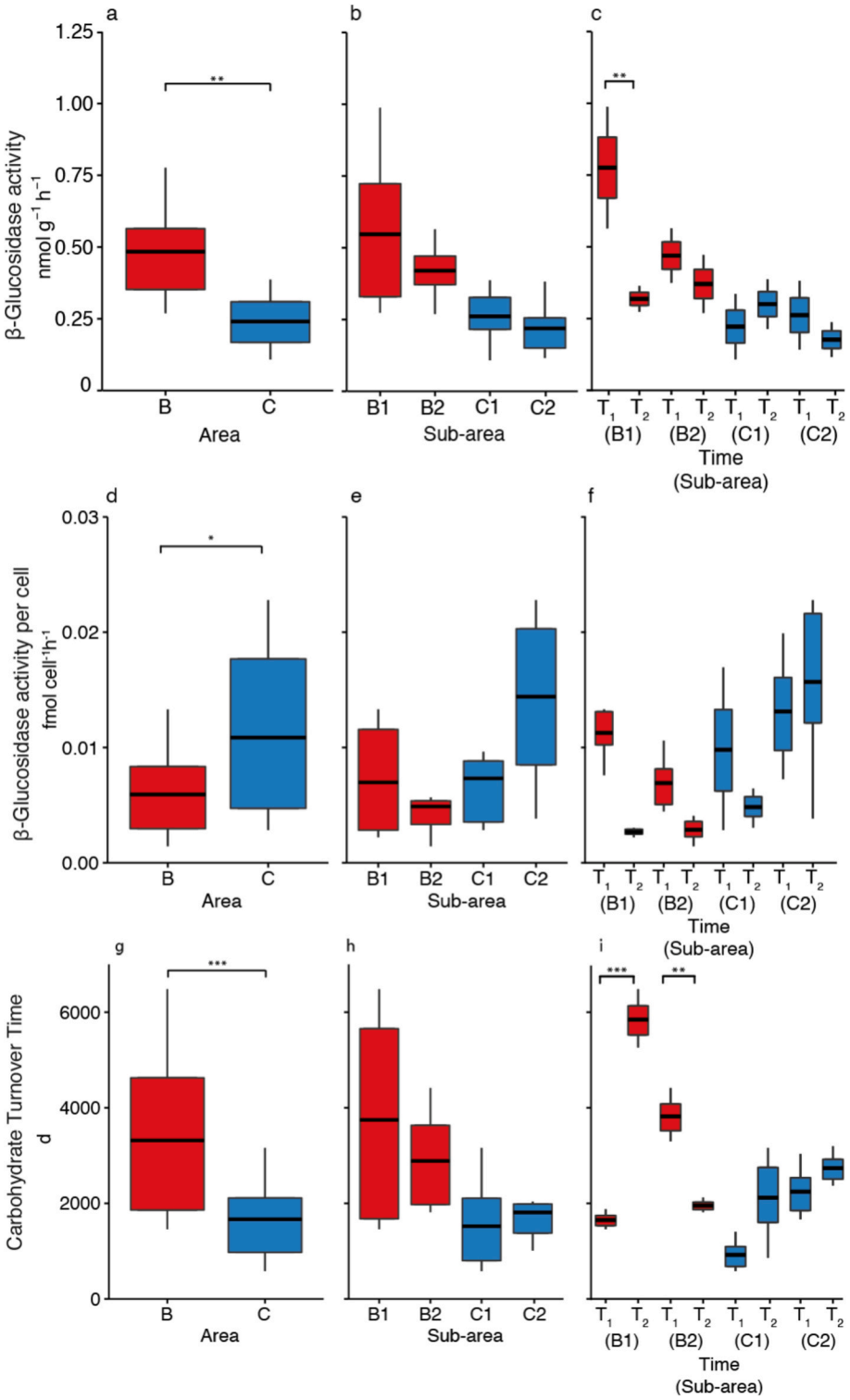

Fig. 5. Spatial and temporal variations of β-glucosidase activity, β-glucosidase activity per cell, and carbohydrate turnover time in the sediments of the two investigated areas. The plots show β-glucosidase activity (expressed as nanomoles of nmol of C hydrolized per gram of dry sediment per hour, nmol $g^{-1}h^{-1}$), cell-specific β-glucosidase activity (expressed as fmol of C hydrolysed per cell per hour, fmol C $cell^{-1}h^{-1}$), and carbohydrate turnover time (expressed as days, d). For each variable, values are shown for the two areas (a, d, g), for the sub-areas within each area (b, e, h), and for the two sampling times within each sub-area (c, f, i). Reported are average values and standard deviations, with asterisks and brackets indicating significant differences found in the pairwise comparisons of PERMANOVA tests (***, $p < 0.001$; **, $p < 0.01$; *, $p < 0.05$).

abundance, $p < 0.01$; AIC = − 30.62; Table 1).

3.4. Viral abundance and production

Viral abundance and viral production were higher in Area B than in C ($p < 0.001$; Table 1), whereas in both areas, viral abundances and

production did not differ between sub-areas nor between sampling periods within each sub-area (Fig. 6). The model selection using the *pooled* approach suggested positive correlations between viral abundance and heterotrophic C production (and biopolymeric carbon concentration) explaining together 87% of the variance (model considering biopolymeric C concentration as predictor variable; $R^2 = 0.866$; heterotrophic carbon production, $p < 0.001$; biopolymeric carbon, $p < 0.01$; AIC = 964.5; Table 1); when considering the bottom-water temperature in the model, positive relationships between viral abundance, heterotrophic C production, and prokaryotic abundance was observed contributing together to 85% of the variance ($R^2 = 0.854$; heterotrophic carbon production, $p < 0.001$; prokaryotic abundance, $p < 0.01$; AIC = 966.5; Table 1).

The *not pooled* approach in the model considering biopolymeric C concentration as predictor variable, revealed a positive relationship between viral and prokaryotic abundance, heterotrophic C production and PRT/CHO ratio in Area B (explaining together 72% of the variance; $R^2 = 0.715$; prokaryotic abundance, $p \leq 0.05$; heterotrophic carbon production, $p < 0.01$; biopolymeric carbon, $p < 0.05$; AIC = 486.7; Table 1), while the model considering bottom-water temperature showed a positive relationship between viral and prokaryotic abundance and a negative relationship with bottom-water temperature (60% of variance explained by all the covariates included; $R^2 = 0.600$; prokaryotic abundance, $p < 0.01$; bottom-water temperature, $p < 0.05$; AIC = 488.7; Table 1). In Area C, the model considering biopolymeric C concentrations as predictor variable showed positive relationships with PRT/CHO ratio and biopolymeric carbon, explaining together 70% of the variance ($R^2 = 0.701$; biopolymeric carbon, $p < 0.01$; PRT/CHO, $p < 0.05$; AIC = 457.6; Table 1), while, when considering bottom-water temperature in the analyses, the regression revealed a relationship with prokaryotic abundance that explained 51% of the variance ($R^2 = 0.508$; prokaryotic abundance, $p < 0.01$; AIC = 461.6; Table 1).

Considering viral production as a response variable, the model selection using the *pooled* approach indicated a positive correlation with heterotrophic C production, explaining 70% of the variance ($R^2 = 0.700$, $p < 0.001$, AIC = 830.8; Table 1). When analysing the two areas separately, the *not pooled* approach revealed positive relationships with heterotrophic C production and prokaryotic abundance and a negative relationship with PRT/CHO ratio in Area B across two models (one considering bottom-water temperature and one considering BPC as predictors; $R^2 = 0.742$; heterotrophic carbon production, $p < 0.01$; prokaryotic abundance, $p < 0.05$; PRT/CHO, $p < 0.05$; AIC = 415.9; Table 1). In addition, the model considering biopolymeric C concentration revealed a positive relationship between viral production and biopolymeric carbon, explaining, together with the other covariates, 96% of the variance ($R^2 = 0.963$; all predictors, $p < 0.001$; AIC = 394.7;

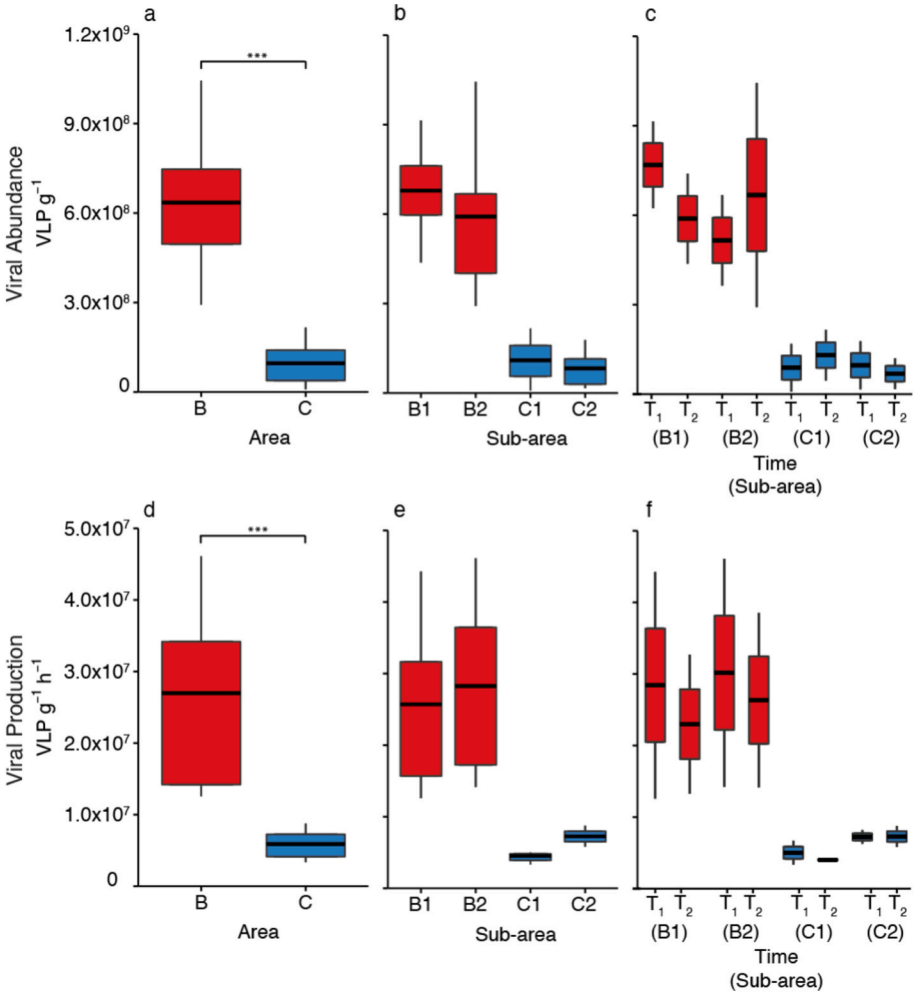

Fig. 6. Spatial and temporal variations of viral abundance and production in the sediments of the two investigated areas. The plots show the viral abundance (expressed as viral-like particles per gram of dry sediment, VLP g^{-1}) and the viral production (expressed as viral-like particles produced per gram of dry sediment per hour, VLP $g^{-1}h^{-1}$) in the two Areas (a, d), in the two sub-areas within each area (b,e), and during the two sampling times within each sub-area (c,f). Reported are average values and standard deviations, with asterisks and brackets indicating significant differences found in the pairwise comparisons of PERMANOVA tests (***, $p < 0.001$; **, $p < 0.01$; *, $p < 0.05$).

Table 1). In Area C, no statistically significant patterns were found, and the best model was the null model (Table 1).

3.5. Prokaryotic diversity based on 16S rRNA gene high-throughput sequencing

A total of 2.779.993 sequences were obtained from the microbial-DNA sequencing (MiSeq Illumina platform). From 15,214 to 70,795 reads per sample were obtained and used by the DADA2 procedure, which infers biologically meaningful ASVs, which were assigned to a total of 56 phyla, 124 classes, 259 orders, and 348 families. The α-diversity analysis showed that the ASV richness was significantly higher in Area C than in B (847 ± 268 ASVs in C *vs* 512 ± 57 ASVs in B; Fig. 7a; $p < 0.01$).

Comparing the sub-areas within each area, significantly higher values of ASV richness in B2 *vs* B1 and in C2 *vs* C1 were found (Fig. 7b; $p < 0.05$). Conversely, comparing times T_1 and T_2 within each sub-area, no significant differences in ASV richness were observed (Fig. 7c). The analysis of ASVs distribution across samples showed that, in terms of ASVs number, 25% of all ASVs were exclusive of Area B (i.e., found in Area B and not in C), 66% were exclusive of Area C, and only 9% were shared between B and C samples (Fig. S4a). The ASVs exclusive of Area B included 1% of core ASVs (i.e., ASVs found in all B samples), 10% of ASVs shared among two or more (but not all) B samples, and 14% of ASVs, exclusive to single B samples (i.e., occurring in only one of the B samples) (Fig. S4a). The ASVs exclusive to Area C included 1.2% of core ASVs (i.e., ASVs found in all C samples), 23% of ASVs shared among two or more (but not all) C samples, and 42% of ASVs exclusive to single C samples (Fig. S4a).

The ASVs shared between B and C samples included only 0.2% ASVs, always found in all analysed samples (Fig. S4a), and 9% ASVs shared between B and C (but not all) samples. The large number of exclusive ASVs within area B or C was represented by a relatively low percentage of 16S rDNA reads (overall, 6% for B and 11% for C). Notably, in Area B, the ASVs shared between B and C samples contributed to the largest portion of the total 16S rDNA reads (48%), while, in Area C, the exclusive ASVs represented the major portion of the reads (44%) (Fig. S4b).

The analysis of the patterns of ASV diversity across samples showed that the prokaryotic assemblages of Area B clustered separately from those of Area C (PERMANOVA; $p < 0.001$; Sorensen's index: 0.87 ± 0.03; Fig. 8a). Samples from Area B clustered neither by sub-area nor by sampling time, while samples from the Area C grouped by sub-area (C1 or C2, PERMANOVA; $p < 0.001$; Sorensen's index: 0.61 ± 0.10), and only samples from C2 clustered by sampling time T_1 or T_2 (PERMANOVA; $p < 0.001$; Sorensen's index: 0.65 ± 0.04; Fig. 8a).

The taxonomic analyses both at the ASV and family level, showed clear segregation between the prokaryotic assemblages of Area B and C, regardless of the spatial or temporal scale (Fig. 8a, b). Proteobacteria dominated in both Areas and were mainly represented by the classes Gammaproteobacteria and Alphaproteobacteria. Gammaproteobacteria were dominated by the Woeseiaceae family (Fig. 8c, Fig. S5). Planctomycetes represented the second most abundant phylum in both Areas, followed by Bacteroidota, dominated by Pirellulaceae. Archaea were dominated by taxa belonging to the family Nitrosopumilaceae (Fig. S5). The abundances of prokaryotic families were different between the two areas, with taxa such as the Rubritaleaceae, Rhodobacteraceae, Dadabacteriales, NB1-j and Kilonellaceae being more relevant in Area B (ANCOM-BC, $p < 0.05$), whereas taxa such as Cyclobacteraceae, Microtrichaceae, pltb-vmat-80 and Thermoanaerobaculaceae were more abundant in Area C (ANCOM-BC, $p < 0.05$ and $q < 0.05$; Fig. 8c, Fig. S6).

The results of the multivariate multiple regression analyses (DistLM forward) carried out in the two Areas (*pooled* approach) on prokaryotic diversity at family level revealed that the biopolymeric C concentration explained alone ca. 55% of the variance (DISTLM $p < 0.001$; Table S5) while taking into account the bottom-water temperature we observe that it accounted for 62.5% of the variance (DISTLM $p < 0.001$; Table S5). No significant results were observed for the *not pooled* approach.

The univariate multiple linear regression selected (with the *pooled* approach) highlighted a negative relationship between the observed ASVs and biopolymeric C concentration which explained 48% of the variance (Table 1). Exploring this relationship with the *not pooled* approaches, biopolymeric C was negatively correlated with the observed ASVs in Area B (50% of the variance), while considering Area C, in addition to biopolymeric C concentration, the variance was also explained by organic matter quality (as PRT/CHO ratio; 72% together).

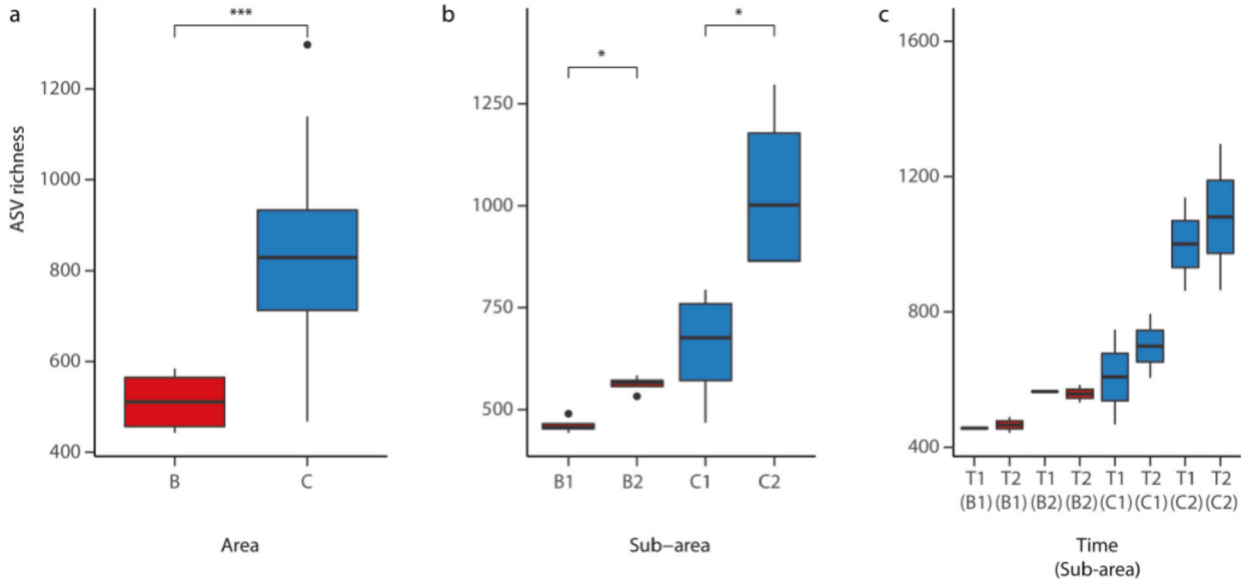

Fig. 7. Spatial and temporal variations of prokaryotic ASV richness in the sediments of the two investigated areas. The plots show ASV richness, expressed as number of observed ASVs, in the two areas (a), in the two sub-areas within each area (b), and during the two sampling times within each sub-area (c). Reported are average values and standard deviations, with asterisks and brackets indicating significant differences found in the pairwise comparisons of statistical tests (***, $p < 0.001$; **, $p < 0.01$; *, $p < 0.05$).

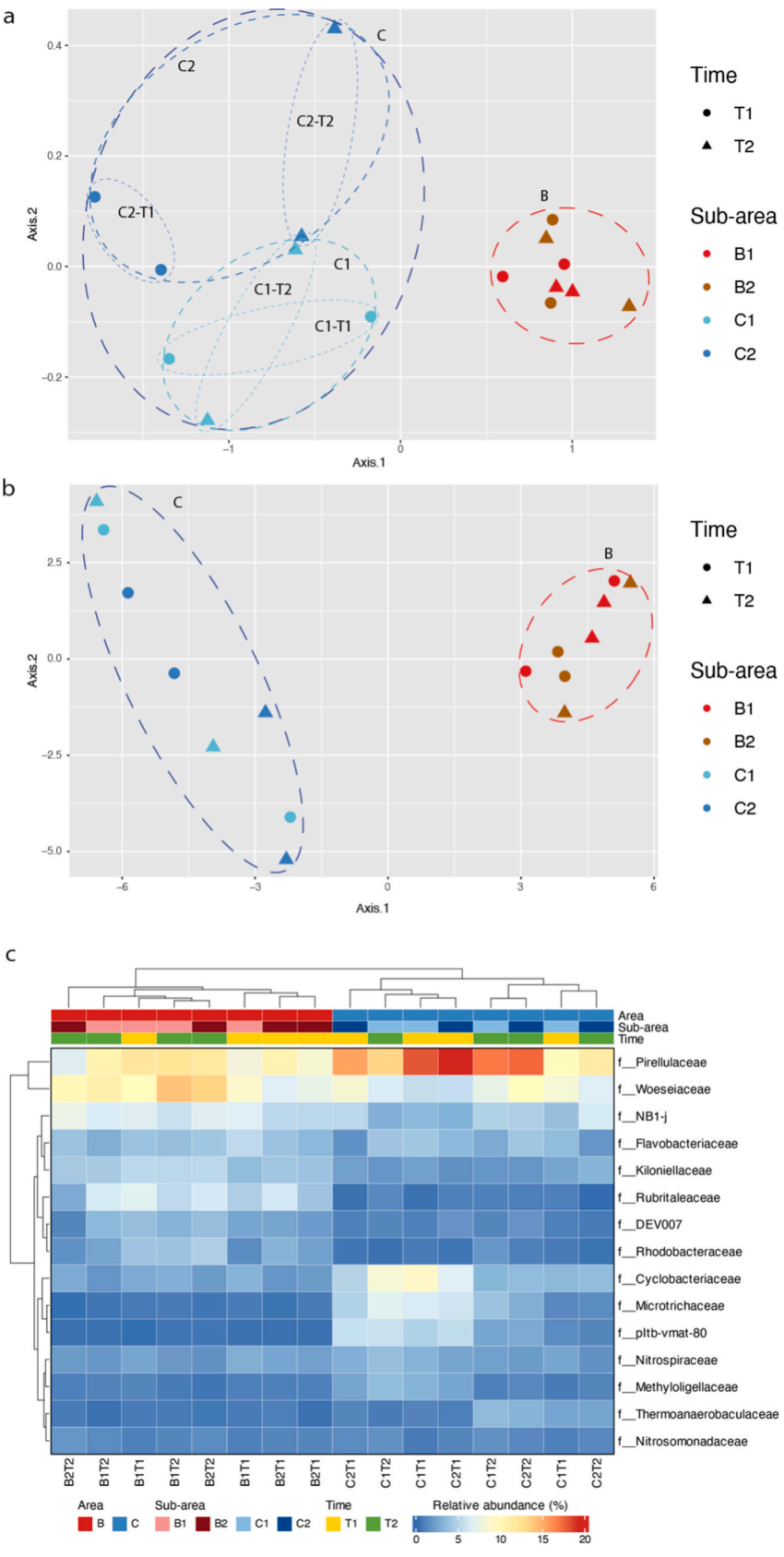

(caption on next page)

Fig. 8. Results of taxonomic analysis. a) PCoA plot representing inter-sample distances calculated using the Aitchison's distance at ASV level. Sample points are coloured according to each subarea, while point shapes are defined according to the sampling time. Ellipses delineate clusters for which PERMANOVA-based statistical analyses showed significant (p-values < 0.05) differences. b) PCoA plot representing inter-sample distances calculated at family level after rarefaction at 15,000 sequences. Sample points are colored according to each sub-area, while point shapes are defined according to the sampling time. c) Heatmap of the top 15 most abundant prokaryotic families selected from the ANCOM-BC-based differential abundance analysis. These families accounted for approximately 80% of the cumulative relative abundance of the differentially abundant families. Heatmap tiles are coloured according to relative abundance (%), from low values in blue to high values in red. Rows represent family-level taxa, whereas columns represent samples. Dendrograms group families and samples according to similarities in their relative-abundance profiles. Annotation bars indicate Area, Sub-area, and Time.

4. Discussion

Organic matter availability and trophic status of the two areas

Understanding the factors influencing microbial-driven ecological processes in Antarctica is crucial for gaining insights into the response of these vulnerable ecosystems to environmental shifts and climate change (Fonseca et al., 2022). Here, we investigated the interactions between different microbial components (bacterial and archaeal diversity), their functions (heterotrophic carbon production, enzymatic activities), and virus-host interactions in two deep-sea Antarctic areas characterized by different levels of primary productivity (and sedimentary organic matter availability) and bottom-water temperature (Δ ca. 1.3°C).

All variables used to describe the trophic conditions of the two areas (organic matter quality, quantity, and phytopigment contents) showed values 5–15 times higher in the colder Area B than in warmer Area C. Such differences were consistent both in time and space and reflected the temporal and spatial gradients of carbon export from the photic zone to the deep sea (Cerchierini et al., 2004; Langone et al., 2000). Both satellite data and direct measurements of the phytopigments deposited on the surface of deep-sea sediments, which are a good proxy of the export of primary organic matter from the photic zone (Pusceddu et al., 2009), confirm the significant differences in phytoplankton C export between the two areas, with larger and higher quality inputs in Area B. All these results suggest that the deep-sea Area B was characterized by mesotrophic conditions, whereas the nearly equally deep seafloor of Area C can be classified as oligotrophic (Pusceddu et al., 2009).

Potential drivers of benthic prokaryotes and viral dynamics in Antarctic sediments

Benthic prokaryotes are strongly influenced by the availability of organic resources, which provide both substrate for metabolism and carbon sources for biomass production (Corinaldesi, 2015; Suttle, 2007). The comparison between the two investigated areas confirmed this relationship: in the mesotrophic Area B, the higher concentration of sedimentary organic matter was accompanied by higher prokaryotic abundance, biomass, and heterotrophic C production, with values generally two- to ten-fold higher than in Area C. Rather than reflecting a uniform increase in all microbial processes, these differences indicate that mesotrophic conditions of Area B were mainly associated with larger prokaryotic standing stock and higher carbon production. Conversely, the more oligotrophic Area C was characterized by higher aminopeptidase activity and faster protein turnover despite lower protein concentrations. This pattern leaves open the question of whether aminopeptidase activity was favoured by warmer bottom-water conditions in the more oligotrophic sediments or, conversely, constrained by the high protein concentrations observed in Area B (Fabiano and Danovaro, 1998).

The contrast observed in prokaryotic biomass, carbon production, and protein turnover also provides a framework for interpreting the observed viral patterns, particularly in relation to the availability of prokaryotic hosts. Viral abundance and production were higher in Area B, where prokaryotic abundance and heterotrophic carbon production reached the highest values. This spatial pattern is consistent with a close association between viral dynamics and the prokaryotic compartment, as prokaryotes represent the main hosts for benthic viruses (Danovaro et al., 2008; Suttle, 2007). In sediments with higher organic matter availability, larger prokaryotic standing stocks and higher heterotrophic production may provide more favourable conditions for viral replication, as viral production is closely linked to the availability and metabolism of prokaryotic hosts (Corinaldesi, 2015; Danovaro et al., 2016a).

At the same time, viral infections can contribute to microbial turnover through host-cell lysis, releasing cellular material into the surrounding sediments and potentially contributing to the recycling of organic compounds within the sedimentary microbial loop (Corinaldesi, 2015; Corinaldesi et al., 2012). This process may be particularly relevant in more oligotrophic sediments, where virus-induced release of labile organic matter could contribute to sustaining extracellular enzymatic processes despite lower bulk organic matter concentrations. Accordingly, the positive relationships between viral production, heterotrophic carbon production, and aminopeptidase activities observed in this study are consistent with an association between viral dynamics and benthic microbial processes involved in organic matter cycling on the Antarctic seafloor.

Prokaryotic biodiversity in the two areas

Our results indicate that sedimentary OM and bottom-water temperature were key environmental factors structuring prokaryotic communities in the two areas. These results confirm previous studies on the role of food supply and temperature on microbial assemblages (Fonseca et al., 2022; Learman et al., 2016). Indeed, although both Areas were dominated by Proteobacteria, they shared only 9.2% of prokaryotic taxa (i.e., ASVs). This low overlap in terms of ASVs indicates that the two areas hosted largely distinct benthic prokaryotic assemblages, with many ASVs occurring only in one of the two areas rather than being shared between them. The consistency of this pattern across sampling times and spatial scales further suggests that the observed turnover in ASV composition did not reflect transient temporal variability or local-scale heterogeneity alone, but rather a stable differentiation between the benthic prokaryotic assemblages of the two areas.

The presence of different taxa in different areas could support the hypothesis of a *niche-driven pattern,* which has been previously reported for Antarctic shallow-water sediments (Fonseca et al., 2022). Here, the distinct benthic prokaryotic communities observed in Area B and Area C may reflect not only spatial separation but also the contrasting environmental conditions characterizing each area (Li et al., 2020). These conditions could favour taxa adapted to different types of organic substrates (Chen et al., 2023; Currie et al., 2021), from the rapid use of more labile compounds in the organic matter-rich Area B to the exploitation of more diverse or complex carbon sources under the more oligotrophic conditions of Area C.

Prokaryotic richness, expressed here as the number of observed ASVs, showed a negative relationship with biopolymeric C and observed ASVs, which suggests that taxonomic richness was lower under OM-rich conditions compared to the more oligotrophic area. In the colder, organic matter-rich Area B, the greater availability of organic substrates may have favoured a more restricted set of taxa specialized in the rapid use of relatively labile organic matter. Under these conditions, fewer taxa may have become numerically dominant, supporting higher microbial standing stocks and heterotrophic C production while reducing overall taxonomic richness (Currie et al., 2021; Gonzalez et al., 2023).

This pattern is consistent with the higher relevance of

Rhodobacteraceae in Area B, a family frequently associated with phytoplankton-derived organic matter and the use of labile algal substrates, as well as with the occurrence of Rubritaleaceae among the taxa most represented in samples characterized by higher organic matter concentrations (Buchan et al., 2014; Ruff et al., 2014). At the same time, the higher ASV richness observed in the warmer and more oligotrophic Area C may reflect the coexistence of taxa able to exploit a broader range of organic substrates. Under more oligotrophic conditions, differences in substrate affinity and degradation capacities could contribute to maintaining a more diversified assemblage. This is consistent with the higher presence in Area C of taxa able to use different carbon sources and degrade complex polysaccharides, such as Cyclobacteriaceae (Krüger et al., 2019) and Hyphomicrobiaceae (Xu, 2014).

Taken together, these findings indicate that higher OM availability may support larger microbial standing stocks, heterotrophic C production, and faster prokaryotic turnover, whereas more oligotrophic conditions may favour the coexistence of a more taxonomically diversified assemblage, potentially reflecting a broader range of strategies for using the available organic substrates.

5. Conclusion

By comparing two Antarctic deep-sea areas characterized by contrasting conditions, this study provides an ecological framework to examine how benthic prokaryotic assemblages, and viral dynamics respond to different environmental settings. Within this framework, our results show that differences in organic matter availability and bottom-water temperature are closely linked to distinct benthic prokaryotic assemblages, metabolic functioning, and virus–host dynamics in Antarctic deep-sea sediments. The colder and organic matter-rich Area B was mainly associated with larger prokaryotic standing stocks, higher heterotrophic carbon production, enhanced β-glucosidase activity, and higher viral production, whereas the warmer and more oligotrophic Area C showed higher prokaryotic ASV richness and faster potential protein degradation. The presence of a small fraction of ASVs shared between the two areas further highlights the ecological differentiation between Area B and Area C, also in terms of prokaryotic assemblages.

Overall, our results highlight that contrasting benthic environmental conditions are closely linked to differences in Antarctic microbial components and organic matter degradation processes. Although this comparison cannot be used to predict microbial responses to future climate-related environmental changes in Antarctica, it provides evidence that shifts in carbon export, trophic conditions, and bottom-water temperature may affect prokaryotic community composition, organic matter degradation, and carbon cycling on the Antarctic seafloor.

CRediT authorship contribution statement

G. Luongo: Writing – review & editing, Writing – original draft, Visualization, Methodology, Investigation, Formal analysis, Data curation, Conceptualization. **C. Corinaldesi:** Writing – review & editing, Visualization, Supervision, Funding acquisition, Conceptualization. **A. Dell'Anno:** Writing – review & editing, Resources, Funding acquisition, Conceptualization. **A. Giorgetti:** Software, Data curation, Conceptualization. **A. Pusceddu:** Formal analysis, Data curation. **E. Rastelli:** Validation, Supervision, Methodology, Investigation, Data curation, Conceptualization. **M. Tangherlini:** Investigation, Formal analysis. **A. Cau:** Formal analysis, Data curation. **C. Ennas:** Formal analysis, Data curation. **S. Greco:** Supervision, Resources. **R. Danovaro:** Writing – review & editing, Validation, Supervision, Project administration, Funding acquisition, Data curation, Conceptualization.

Declaration of competing interest

The authors declare that they have no known competing financial interests or personal relationships that could have appeared to influence the work reported in this paper.

Acknowledgments

This study was carried out in the framework of the BEDROSE (PNRA) and VIRIDE projects (PRIN 2017, n. 2017EKFA98) financially supported by the Ministry of University and Research. The authors thank all the crew members for supporting sample collection. This study was supported by the National Recovery and Resilience Plan (NRRP), Mission 4 Component 2 Investment 1.4—Call for tender no. 3138 of 16 December 2021, rectified by Decree no. 3175 of 18 December 2021 by the Italian Ministry of University and Research, funded by the Next-GenerationEU, Award Number: project code CN_00000033, Concession Decree No. 1034, of 17 June 2022, adopted by the Italian Ministry of University and Research, Project title "National Biodiversity Future Center—NBFC".

Appendix A. Supplementary data

Supplementary data to this article can be found online at https://doi.org/10.1016/j.pocean.2026.103792.

Data availability

Data of raw sequencing reads have been deposited in the NCBI Sequence Read Archive (SRA) within the BioProject PRJNA836760. Satellite data of net primary production can be downloaded from the Copernicus Marine Service (CMEMS) database (https://doi.org/10.48670/moi-00281).

All data needed to evaluate the conclusions in the paper are present in the paper and/or the Supplementary Materials. Additional data related to this paper may be requested from the authors.

References

Anderson, M.J., 2014. Permutational multivariate analysis of variance (PERMANOVA). Wiley Statsref: Statistics Reference Online 1–15.
Anderson, M.J., Millar, R.B., 2004. Spatial variation and effects of habitat on temperate reef fish assemblages in northeastern New Zealand. J. Exp. Mar. Biol. Ecol. 305 (2), 191–221.
Arneth, A., Shin, Y.-J., Leadley, P., Rondinini, C., Bukvareva, E., Kolb, M., Midgley, G.F., Oberdorff, T., Palomo, I., Saito, O., 2020. Post-2020 biodiversity targets need to embrace climate change. Proc. Natl. Acad. Sci. 117 (49), 30882–30891.
Arrigo, K.R., van Dijken, G.L., Bushinsky, S., 2008. Primary production in the Southern Ocean, 1997–2006. J. Geophys. Res. Oceans 113 (C8).
Arteaga, L.A., Boss, E., Behrenfeld, M.J., Westberry, T.K., Sarmiento, J.L., 2020. Seasonal modulation of phytoplankton biomass in the Southern Ocean. Nat. Commun. 11 (1), 5364.
Bligh, E.G., Dyer, W.J., 1959. A rapid method of total lipid extraction and purification. Can. J. Biochem. Physiol. 37 (8), 911–917.
Bolinesi, F., Saggiomo, M., Ardini, F., Castagno, P., Cordone, A., Fusco, G., Rivaro, P., Saggiomo, V., Mangoni, O., 2020. Spatial-related community structure and dynamics in phytoplankton of the Ross Sea. Antarctica. Frontiers in Marine Science 7, 574963.
Bolyen, E., Rideout, J.R., Dillon, M.R., Bokulich, N.A., Abnet, C.C., Al-Ghalith, G.A., Alexander, H., Alm, E.J., Arumugam, M., Asnicar, F., 2019. Reproducible, interactive, scalable and extensible microbiome data science using QIIME 2. Nat. Biotechnol. 37 (8), 852–857.
Buchan, A., LeCleir, G.R., Gulvik, C.A., González, J.M., 2014. Master recyclers: features and functions of bacteria associated with phytoplankton blooms. Nat. Rev. Microbiol. 12 (10), 686–698.
Capotondi, L., Bonomo, S., Budillon, G., Giordano, P., Langone, L., 2020. Living and dead benthic foraminiferal distribution in two areas of the Ross Sea (Antarctica). Rend. Lincei Sci. Fis. Nat. 31, 1037–1053.
Cerchierini, M., Langone, L., Ravaioli, M., Ismar-cnr, s.g.m.,, 2004. Sediment trap particle fluxes in the Northwestern Ross sea, Antarctica. Atti Assoc Ital Oceanol Limnol 17, 13–17.
Chen, X., Cai, R., Zhuo, X., Chen, Q., He, C., Sun, J., Zhang, Y., Zheng, Q., Shi, Q., Jiao, N., 2023. Niche differentiation of microbial community shapes vertical distribution of recalcitrant dissolved organic matter in deep-sea sediments. Environ. Int. 178, 108080.
Chiarini, F., Ravaioli, M., Capotondi, L., 2019. Interannual variability of vertical particle fluxes in the Ross Sea (Antarctica). Nat. Conserv. 34, 417–440.
Comiso, J.C., 2010. Variability and trends of the global sea ice cover. Sea Ice 2, 205–246.
Corinaldesi, C., 2015. New perspectives in benthic deep-sea microbial ecology. Front. Mar. Sci. 2, 17.

Corinaldesi, C., Dell'Anno, A., Danovaro, R., 2012. Viral infections stimulate the metabolism and shape prokaryotic assemblages in submarine mud volcanoes. ISME J. 6 (6), 1250–1259.
Currie, A.A., Marshall, A.J., Lohrer, A.M., Cummings, V.J., Seabrook, S., Cary, S.C., 2021. Sea ice dynamics drive benthic microbial communities in McMurdo Sound. Antarctica. Frontiers in Microbiology 12, 745915.
Danovaro, R., 2009. Methods for the study of deep-sea sediments, their functioning and biodiversity. CRC Press.
Danovaro, R., Corinaldesi, C., Dell'Anno, A., Rastelli, E., 2017. Potential impact of global climate change on benthic deep-sea microbes. FEMS Microbiol. Lett. 364 (23), fnx214.
Danovaro, R., Corinaldesi, C., Rastelli, E., Anno, A.D., 2015. Towards a better quantitative assessment of the relevance of deep-sea viruses, Bacteria and Archaea in the functioning of the ocean seafloor. Aquat. Microb. Ecol. 75 (1), 81–90.
Danovaro, R., Dell'Anno, A., Corinaldesi, C., Magagnini, M., Noble, R., Tamburini, C., Weinbauer, M., 2008. Major viral impact on the functioning of benthic deep-sea ecosystems. Nature 454 (7208), 1084–1087.
Danovaro, R., Dell'Anno, A., Corinaldesi, C., Rastelli, E., Cavicchioli, R., Krupovic, M., Noble, R.T., Nunoura, T., Prangishvili, D., 2016a. Virus-mediated archaeal hecatomb in the deep seafloor. Sci. Adv. 2 (10), e1600492.
Danovaro, R., Molari, M., Corinaldesi, C., Dell'Anno, A., 2016b. Macroecological drivers of archaea and bacteria in benthic deep-sea ecosystems. Sci. Adv. 2 (4), e1500961.
Danovaro, R., Snelgrove, P.V., Tyler, P., 2014. Challenging the paradigms of deep-sea ecology. Trends Ecol. Evol. 29 (8), 465–475.
Dell'Anno, A., Corinaldesi, C., Magagnini, M., Danovaro, R., 2009. Determination of viral production in aquatic sediments using the dilution-based approach. Nat. Protoc. 4 (7), 1013–1022.
Fabiano, M., Danovaro, R., 1998. Enzymatic activity, bacterial distribution, and organic matter composition in sediments of the Ross Sea (Antarctica). Appl. Environ. Microbiol. 64 (10), 3838–3845.
Fonseca, V., Kirse, A., Giebner, H., Vause, B., Drago, T., Power, D., Peck, L., Clark, M., 2022. Metabarcoding the Antarctic Peninsula biodiversity using a multi-gene approach. ISME Commun. 2 (1), 37.
Garnesson, P., Mangin, A., Fanton d'Andon, O., Demaria, J., Bretagnon, M., 2019. The CMEMS GlobColour chlorophyll a product based on satellite observation: Multi-sensor merging and flagging strategies. Ocean Sci. 15 (3), 819–830.
Gerchakov, S.M., Hatcher, P.G., 1972. Improved technique for analysis of carbohydrates in sediments 1. Limnol. Oceanogr. 17 (6), 938–943.
Gloor, G.B., Macklaim, J.M., Pawlowsky-Glahn, V., Egozcue, J.J., 2017. Microbiome datasets are compositional: and this is not optional. Front. Microbiol. 8, 2224.
Gonzalez, S.V., Dafforn, K.A., Gribben, P.E., O'Connor, W.A., Johnston, E.L., 2023. Organic enrichment reduces sediment bacterial and archaeal diversity, composition, and functional profile independent of bioturbator activity. Mar. Pollut. Bull. 196, 115608.
Halberstadt, A.R.W., Simkins, L.M., Greenwood, S.L., Anderson, J.B., 2016. Past ice-sheet behaviour: retreat scenarios and changing controls in the Ross Sea. Antarctica. the Cryosphere 10 (3), 1003–1020.
Hartree, E.F., 1972. Determination of protein: a modification of the Lowry method that gives a linear photometric response. Anal. Biochem. 48 (2), 422–427.
Jacobs, S., Giulivi, C., Dutrieux, P., 2022. Persistent Ross Sea freshening from imbalance West Antarctic ice shelf melting. J. Geophys. Res. Oceans 127 (3), e2021JC017808.
Jacobs, S.S., Fairbanks, R.G., Horibe, Y., 1985. Origin and evolution of water masses near the Antarctic continental margin: evidence from H218O/H216O ratios in seawater. Oceanology of the Antarctic Continental Shelf 43, 59–85.
Jones, D.O., Yool, A., Wei, C.L., Henson, S.A., Ruhl, H.A., Watson, R.A., Gehlen, M., 2014. Global reductions in seafloor biomass in response to climate change. Glob. Chang. Biol. 20 (6), 1861–1872.
Krüger, K., Chafee, M., Ben Francis, T., Glavina del Rio, T., Becher, D., Schweder, T., Amann, R.I., Teeling, H., 2019. In marine Bacteroidetes the bulk of glycan degradation during algae blooms is mediated by few clades using a restricted set of genes. ISME J. 13 (11), 2800–2816.
Langone, L., Frignani, M., Ravaioli, M., Bianchi, C., 2000. Particle fluxes and biogeochemical processes in an area influenced by seasonal retreat of the ice margin (northwestern Ross Sea, Antarctica). J. Mar. Syst. 27 (1–3), 221–234.
Learman, D.R., Henson, M.W., Thrash, J.C., Temperton, B., Brannock, P.M., Santos, S.R., Mahon, A.R., Halanych, K.M., 2016. Biogeochemical and microbial variation across 5500 km of Antarctic surface sediment implicates organic matter as a driver of benthic community structure. Front. Microbiol. 7, 284.
Li, J., Gu, X., Gui, Y., 2020. Prokaryotic diversity and composition of sediments from Prydz Bay, the Antarctic peninsula region, and the Ross Sea, southern ocean. Front. Microbiol. 11, 783.
Lorenzen, Carl, J., Shirley, Winifred Jeffrey., 1980. Determination of chlorophyll in seawater. Report of intercalibration tests. In: *UNESCO Technical Papers in Marine Science= Documents techniques de l'Unesco sur les sciences*. de la mer.
Mangoni, O., Saggiomo, V., Bolinesi, F., Escalera, L., Saggiomo, M., 2018. A review of past and present summer primary production processes in the Ross Sea in relation to changing ecosystems. Ecol. Quest. 29 (3), 75–85.
Mangoni, O., Saggiomo, V., Bolinesi, F., Margiotta, F., Budillon, G., Cotroneo, Y., Misic, C., Rivaro, P., Saggiomo, M., 2017. Phytoplankton blooms during austral summer in the Ross Sea, Antarctica: Driving factors and trophic implications. PLoS One 12 (4), e0176033.
Marsh, J.B., Weinstein, D.B., 1966. Simple charring method for determination of lipids. J. Lipid Res. 7 (4), 574–576.
Martino, C., Morton, J.T., Marotz, C.A., Thompson, L.R., Tripathi, A., Knight, R., Zengler, K., 2019. A novel sparse compositional technique reveals microbial perturbations. Msystems 4 (1), 00016-00019. https://doi.org/10.1128/msystems.
McArdle, B.H., Anderson, M.J., 2001. Fitting multivariate models to community data: a comment on distance-based redundancy analysis. Ecology 82 (1), 290–297.
McKinney, W., 2011. pandas: a foundational Python library for data analysis and statistics. Python for High Performance and Scientific Computing 14 (9), 1–9.
Nomaki, H., Rastelli, E., Alves, A., Suga, H., Ramos, S., Kitahashi, T., Tsuchiya, M., Ogawa, N.O., Matsui, Y., Seike, K., 2021. Abyssal fauna, benthic microbes, and organic matter quality across a range of trophic conditions in the western Pacific ocean. Prog. Oceanogr. 195, 102591.
Orsi, A.H., Wiederwohl, C.L., 2009. A recount of Ross Sea waters. Deep Sea Res. Part II 56 (13–14), 778–795.
Parada, A.E., Needham, D.M., Fuhrman, J.A., 2016. Every base matters: assessing small subunit rRNA primers for marine microbiomes with mock communities, time series and global field samples. Environ. Microbiol. 18 (5), 1403–1414.
Pusceddu, A., Dell'Anno, A., Fabiano, M., Danovaro, R., 2009. Quantity and bioavailability of sediment organic matter as signatures of benthic trophic status. Mar. Ecol. Prog. Ser. 375, 41–52.
Quast, C., Pruesse, E., Yilmaz, P., Gerken, J., Schweer, T., Yarza, P., Peplies, J., Glöckner, F.O., 2012. The SILVA ribosomal RNA gene database project: improved data processing and web-based tools. Nucleic Acids Res. 41 (D1), D590–D596.
Queirós, J.P., Borras-Chavez, R., Friscourt, N., Groß, J., Lewis, C.B., Mergard, G., O'Brien, K., 2024. Southern Ocean food-webs and climate change: a short review and future directions. PLOS Clim. 3 (3), e0000358.
Rice, D.L., 1982. The detritus nitrogen problem: new observations and perspectives from organic geochemistry. Mar. Ecol. Prog. Ser. 9, 153–162.
Rivaro, P., Messa, R., Ianni, C., Magi, E., Budillon, G., 2014. Distribution of total alkalinity and pH in the Ross Sea (Antarctica) waters during austral summer 2008. Polar Res. 33 (1), 20403.
Ruff, S.E., Probandt, D., Zinkann, A.-C., Iversen, M.H., Klaas, C., Würzberg, L., Krombholz, N., Wolf-Gladrow, D., Amann, R., Knittel, K., 2014. Indications for algae-degrading benthic microbial communities in deep-sea sediments along the Antarctic Polar Front. Deep Sea Res. Part II 108, 6–16.
Silvano, A., Foppert, A., Rintoul, S.R., Holland, P.R., Tamura, T., Kimura, N., Castagno, P., Falco, P., Budillon, G., Haumann, F.A., 2020. Recent recovery of Antarctic Bottom Water formation in the Ross Sea driven by climate anomalies. Nat. Geosci. 13 (12), 780–786.
Smith, C.R., De Leo, F.C., Bernardino, A.F., Sweetman, A.K., Arbizu, P.M., 2008. Abyssal food limitation, ecosystem structure and climate change. Trends Ecol. Evol. 23 (9), 518–528.
Smith Jr, W.O., Ainley, D.G., Arrigo, K.R., Dinniman, M.S., 2014. The oceanography and ecology of the Ross Sea. Ann. Rev. Mar. Sci. 6, 469–487.
Smith, W.O., Comiso, J.C., 2009. Southern ocean primary productivity: Variability and a view to the future. Contributions to International Polar Year Science, Smithsonian at the Poles.
Suttle, C.A., 2007. Marine viruses—major players in the global ecosystem. Nat. Rev. Microbiol. 5 (10), 801–812.
Sweetman, A.K., Smith, C.R., Shulse, C.N., Maillot, B., Lindh, M., Church, M.J., Meyer, K. S., van Oevelen, D., Stratmann, T., Gooday, A.J., 2019. Key role of bacteria in the short-term cycling of carbon at the abyssal seafloor in a low particulate organic carbon flux region of the eastern Pacific Ocean. Limnol. Oceanogr. 64 (2), 694–713.
Sweetman, A.K., Thurber, A.R., Smith, C.R., Levin, L.A., Mora, C., Wei, C.-L., Gooday, A. J., Jones, D.O., Rex, M., Yasuhara, M., 2017. Major impacts of climate change on deep-sea benthic ecosystems. Elem. Sci. Anth. 5, 4.
Thullner, M., Regnier, P., 2019. Microbial controls on the biogeochemical dynamics in the subsurface. Rev. Mineral. Geochem. 85 (1), 265–302.
Walker, A.M., Leigh, M.B., Mincks, S.L., 2021. Patterns in benthic microbial community structure across environmental gradients in the beaufort sea shelf and slope. Front. Microbiol. 37.
Whitman, W.B., Coleman, D.C., Wiebe, W.J., 1998. Prokaryotes: the unseen majority. Proc. Natl. Acad. Sci. 95 (12), 6578–6583.
Xu, A.-O.-X.-W., 2014. The Family Hyphomicrobiaceae. 11 the Family Hyphomicrobiaceae, 11.
Zuur, A.F., Ieno, E.N., 2016. A protocol for conducting and presenting results of regression-type analyses. Methods Ecol. Evol. 7 (6), 636–645.